J. Fluid Mech. (2006), *vol.* 547, *pp.* 231–256.
doi:10.1017/S0022112005007329 Printed in the United Kingdom

On the nonlinear water entry problem of asymmetric wedges

By Yu. A. SEMENOV[1] AND A. IAFRATI[2]

[1]Institute of Hydromechanics of the NAS of Ukraine, Kiev, Ukraine

[2]INSEAN – The Italian Ship Model Basin, Roma, Italy

(Received 4 August 2004 and in revised form 7 July 2005)

The self-similar solution that characterizes the water impact, with a constant vertical velocity, of a wedge entering the free surface with an arbitrary orientation is derived analytically. The study is carried out by assuming the fluid to be ideal, weightless and with negligible surface tension effects. The solution is based on the complex analysis of nonlinear two-dimensional problems of unsteady free boundary flows and is written in terms of two governing functions, which are the complex velocity and the derivative of the complex potential defined in a parameter domain. The boundary value problem is reduced to the system of an integral and an integro-differential equation in terms of the velocity modulus and of the velocity angle to the free surface, both written as functions of a parameter variable. The system of equations is solved through a numerical procedure which is validated in the case of symmetric wedges. Comparisons with data available in literature are established for this purpose. Results are presented in terms of free surface shape, contact angles at the intersection with the wedge boundary, pressure distribution, force and moment coefficients. For a given wedge angle, the changes induced by the heel angle on the above quantities are discussed. A criterion is proposed to determine the limit conditions beyond which flow separation from the wedge apex occurs. Comparisons with experimental results available in literature are presented.

1. Introduction

Water impact problems have several important applications in various aspects of the naval field. Besides their natural connection with ship slamming (Faltinsen, Landrini & Greco 2004) and planing hulls, renewed attention has been given recently to the high-speed hydrodynamics of seaplanes, surface-piercing propellers and the interaction of high-speed liquid drops with structural elements. The short duration and the large unsteady component of the hydrodynamic loads, which may greatly exceed the corresponding steady values, are the main features of water impact processes.

From the mathematical standpoint, water impact problems belong to the class of inverse boundary value problems in which nonlinear and unsteady effects are strongly coupled. Moreover, the solution of water impact flows is complicated by the singularities which occur along the three-phase contact line, that is at the intersection of the free surface with the solid body contour. Historically, progress in solving two-dimensional free boundary potential flows has been made through the development of the theory of complex variable functions. As any analytical function is curl and divergence free, the problem is to find an analytical function, that is the complex potential, which satisfies the boundary conditions.

First attempts to solve this rather complicated problem, mainly focused on the analysis of seaplane landing, were proposed by von Kármán (1929) and Wagner (1932) who considered the water entry process as sequence of impact impulses. Tulin (1957) developed a three-dimensional planing flow theory using a slender-body approximation and solved the linearized problem of the two-dimensional flow in the cross-plane. The complete linearized solution of the water entry of a wedge was first proposed by Mackie (1962). More recently, the Wagner's theory has been generalized to the vertical entry of a horizontal circular cylinder (Armand & Cointe 1987; Cointe 1991). Different simplified models for the wedge entry problem have been also proposed by Howison, Ockendon & Wilson (1991), Fraenkel & Mcleod (1997), and Mei, Liu & Yue (1999).

An exact nonlinear self-similar solution of the water entry problem was obtained by Dobrovol'skaya (1969) for a symmetric wedge entering the free surface vertically and with a constant velocity. Self-similarity is a model of the initial stage of water impact processes with entry velocity large enough to make gravity effects negligible but not high enough to make acoustic effects relevant. These latter effects are of major importance in the impact of very blunt bodies or during the very early stage after the impulsive start of floating bodies (Korobkin & Peregrine 2000). The key point of Dobrovol'skaya's solution is finding Wagner's function from its real value on the whole fluid boundary by using the Schwarz integral and Sokhotsky–Plemelj formula. In this way, the boundary value problem is reduced to a nonlinear singular integral equation. Existence and uniqueness of the similarity solution on the basis of this approach has been proved for all wedge angles (Fraenkel & Keady 2004). Owing to the difficulties related to the singularity at the jet tip, Dobrovol'skaya (1969) solved the singular integral equation numerically only for deadrise angles larger than 30°.

The singularity at the jet tip is also responsible for the difficulties that fully nonlinear numerical approaches, recently developed, encounter when dealing with this rather complicated problem (Greenhow 1987). In order to overcome this difficulty, Zhao & Faltinsen (1993) developed a model to cut the thin jet layer off the computational domain. The model exploits the fact that pressure variations within this region are small. The numerical approach is based on a mixed Eulerian–Lagrangian formulation which accounts for all the nonlinearities in the time integration and makes use of a boundary element method to determine the flow field at each time step. By using this numerical approach they derived the solution for symmetric wedges with deadrise angles ranging from 4° to 81°. Comparisons with results obtained through the Dobrovol'skaya model showed the validity of the assumption made when truncating the thin jet layer. Instead of truncating the thinnest part of the jet, Battistin & Iafrati (2004) developed a hybrid finite-boundary element method which proved to be accurate and efficient. The hybrid method eliminates the intrinsic difficulties that boundary element approaches have in describing the solution within fluid layers thinner than the panel size. In order to avoid difficulties related to the singularity at the jet tip, Wu, Sun & He (2004) proposed an analytical solution for the flow inside the jet based on the shallow water approximation.

In spite of the intense research activity carried out for symmetric wedges, little work has been done on asymmetric water entry although this problem is common in the naval field (Howison, Ockendon & Oliver 2004). As an example, it may occur when vessels undergo vertical motion in the presence of waves. Moreover, such flow conditions occur about planing hulls during manoeuvring operations. The

first models for asymmetric wedge impact within the potential flow theory were proposed by Garabedian (1953) and Borg (1957). More recently, this problem was considered by Korobkin (1988), Chekin (1989), Toyama (1993), and Scolan *et al.* (1999). In Iafrati (2000) a fully nonlinear numerical method has been developed and applied to the prediction of the free-surface shape and of the pressure distribution induced by the vertical water entry of an asymmetric wedge. In Judge, Troesch & Perlin (2004) a careful experimental analysis has been carried out for the asymmetric/oblique water entry of a wedge. The analysis was aimed at investigating the limit conditions beyond which the flow separates from the wedge apex and one side of the wedge remains dry. Besides the experimental analysis, the problem was investigated theoretically through the flat cylinder theory, originally developed by Vorus (1996), and extended to asymmetric configurations in Xu, Troesch & Vorus (1998). Chekin (1989) presented the solution of asymmetric/oblique entry of a wedge obtained through the construction of a function which conformally maps the upper half-plane onto the flow domain using the Schwarz integral and the Sokhotsky–Plemelj formula. The model assumes that flow separation always occurs in asymmetric water entry, although this assumption seems not confirmed by the experiments (Judge *et al.* 2004). The mapping method of complex analysis has been also applied by de Divitiis & de Socio (2002) to the study of asymmetric wedge impact. They built a physico-mathematical model in which the jet tips are represented by sinks and proposed a theoretical expression for the flow potential including several unknown parameters, which are found by using an optimization procedure to enforce mass, momentum and energy conservation. Although they speculate about the dynamic and kinematic boundary conditions, these conditions were not used in the derivation of the results.

In this paper we present a nonlinear analytical self-similar solution of the asymmetric/oblique water entry flow of a wedge which does not assume flow separation from the wedge apex. The solution is given in terms of two governing functions, which are the complex velocity and the derivative of the complex potential defined in the parameter domain. The theoretical formulation of the problem is discussed in § 2 where these governing functions are derived. The complex velocity is written as a function of the variation of the velocity modulus along the free boundary whereas the derivative of the complex potential contains a function representing the angle that the velocity vector forms with the free surface. Both the variation of the velocity modulus and the angle of the velocity vector are functions of a parameter variable along the free surface. By exploiting the self-similarity of the problem and the dynamic and kinematic boundary conditions, the solution is derived in the form of a system of an integral and an integro-differential equation with respect to the aforementioned functions. In § 3 the method of successive approximations adopted for solving the system of integral equations is presented along with a careful validation carried out in the case of the vertical water entry of symmetric wedges. In § 4 solutions obtained for asymmetric wedge impact are presented in terms of free surface shape, contact angle at the tips, pressure distributions and force and moment coefficients. For a fixed wedge angle, results obtained for different heel angles are provided and the role played by the asymmetry in the above quantities is discussed. Particular attention is given to the limit conditions beyond which flow separation from the wedge apex may take place and only one side of the wedge is completely wetted by the liquid. Owing to the assumptions made, these also represent the limits for the applicability of the present model.

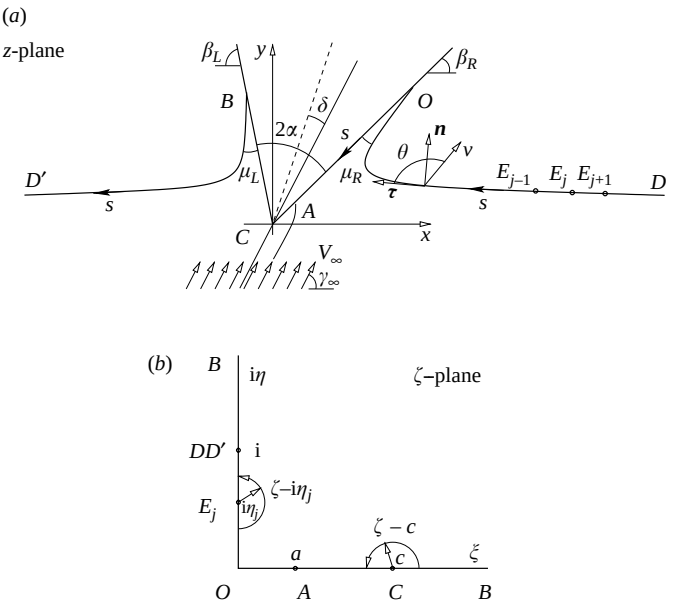

FIGURE 1. Sketches of (*a*) the physical plane and (*b*) the parameter domain with the notations used.

2. Theoretical formulation

The fluid is assumed incompressible and its flow potential with gravity and surface tension effects negligible. The flow about an asymmetric wedge entering a liquid surface, originally at rest, is studied in a frame of reference attached to the impacting body with its origin C located at the wedge apex. The bisector of the wedge is inclined at an angle δ with respect to the velocity of the fluid far from the wedge, which forms an angle γ_∞ with the horizontal axis x and its modulus approaches the value V_∞ (see figure 1*a*). The heel angle δ is positive when the wedge is rotated counterclockwise with respect to the velocity direction. Let 2α denote the wedge angle; it follows that $\beta_L = \pi - \gamma_\infty - \alpha - \delta$ and $\beta_R = \gamma_\infty - \alpha + \delta$ are the deadrise angles with respect to the incoming flow on the left- and right-hand sides, respectively.

For a constant entry velocity, the time-dependent problem in the physical plane $Z = X + \mathrm{i}Y$ can be written in terms of a self-similar solution in a stationary domain $z = x + \mathrm{i}y$, with $x = X/(V_0 t)$, $y = Y/(V_0 t)$ where V_0 is the velocity modulus in the physical plane of the contact point O at the right-hand side of the wedge. According to the above definitions, V_0 is used as a reference value and then the velocity modulus of the point O in the stationary plane is unity ($v_0 = 1$). The complex velocity potential $W(Z, t) = \Phi(Z, t) + \mathrm{i}\Psi(Z, t)$ takes the form

$$W(Z, t) = V_0^2 t\, w(z) = V_0^2 t\, [\phi(z) + \mathrm{i}\psi(z)], \tag{2.1}$$

where ϕ and ψ are the velocity potential and the stream function in the stationary plane z.

The problem is to determine the mapping function from the stationary plane z onto the complex velocity potential domain w. Following Helmholtz (1868) and Kirchhoff (1869), Zhukovskii (1890) proposed a useful method for solving problems of steady

jet flows by introducing the function

$$\omega = -\ln \frac{\mathrm{d}w}{\mathrm{d}z}.$$

Instead of finding the conformal map $w = w(z)$ directly, he mapped an upper half-plane onto both the $\omega(\zeta)$ and $w(\zeta)$ domains. If $\omega(\zeta)$ and $w(\zeta)$ are known in terms of the parameter variable ζ, the velocity field and the mapping function can be determined as follows:

$$\frac{\mathrm{d}w}{\mathrm{d}z} = \exp(-\omega(\zeta)), \qquad z(\zeta) = z(0) + \int_0^{\zeta} \frac{\mathrm{d}w}{\mathrm{d}\zeta} \Big/ \frac{\mathrm{d}w}{\mathrm{d}z}\, \mathrm{d}\zeta. \tag{2.2}$$

Since for steady jet flows past polygonal bodies the map of the fluid domain onto the w-plane and ω-plane has a polygonal shape, the mapping function can be found through the Schwarz–Christoffel formula. Chaplygin, analysing different types of singularities which may occur for various two-dimensional problems, proposed the construction of $\mathrm{d}w/\mathrm{d}z$ and $\mathrm{d}w/\mathrm{d}\zeta$ without introducing the conformal mapping in an explicit form. Instead, several auxiliary parameter regions are considered with the only condition that the boundaries are composed of straight line segments and/or arcs of circles which make the use of mirror images easy. Chaplygin's method is discussed in the book by Gurevich (1965). In contrast to steady flows, in the present free surface flow the velocity modulus varies along the free boundary, thus requiring a different procedure for the construction of the expressions for the complex velocity $\mathrm{d}w/\mathrm{d}z$ and for the derivative of the complex potential $\mathrm{d}w/\mathrm{d}\zeta$.

We choose the first quadrant of the ζ-plane as a parameter domain to obtain the expressions for the derivative of the complex potential and the complex velocity in terms of $\zeta = \xi + \mathrm{i}\eta$. Three arbitrary points are fixed in the parameter domain, which are O, B, and D as shown in figure 1(*b*). In this plane the free surface is along the positive imaginary axis ($\eta > 0, \xi = 0$) whereas the wetted part of the wedge is along the positive real axis ($\xi > 0, \eta = 0$) and the points $\zeta = a$ and $\zeta = c$ correspond to the stagnation point A and to the wedge apex C in the physical plane, respectively. The parameters a and c are unknowns and have to be derived as a part of the solution.

2.1. *Expression for the complex velocity*

In order to derive the expression for the complex velocity, we note that it has two singularities which correspond to the stagnation point A and to the wedge apex C (figure 1) where the velocity field diverges. Furthermore, on the free surface, the velocity modulus changes from $v = 1$ at the contact point O, up to v_∞ at infinity D and, similarly, it varies from v_∞ to v_B when moving from infinity D' to the contact point B lying on the left-hand side of the wedge. At this stage it is assumed that the velocity modulus along the free surface, that is along the imaginary axis,

$$v(\eta) = \left| \frac{\mathrm{d}w}{\mathrm{d}z} \right|,$$

is known. This function is determined later on by using the dynamic boundary condition. Due to the impermeability condition, on the real axis of the parameter domain the argument of the complex conjugate velocity is fixed and is

$$\arg\left(\frac{\mathrm{d}w}{\mathrm{d}z}\right) = \begin{cases} -\beta_R, & 0 < \xi < a \\ \pi - \beta_R, & a < \xi < c \\ -\pi + \beta_L, & c < \xi < \infty. \end{cases} \tag{2.3}$$

The problem is to find the function $\mathrm{d}w/\mathrm{d}z$ in the parameter domain which satisfies the given boundary conditions. With the aim of applying the singular points method, we decompose the free boundary into N intervals (E_{j-1}, E_j), with $j = 1$–N, and assume that the velocity modulus is piecewise constant, that is $v(\eta) = v_j$ for $\eta \in (\eta_{j-1}, \eta_j)$, so that the velocity modulus changes stepwise from v_{j-1} to v_j at each vertex E_{j-1}. Here $\eta_0 = 0$ and $\eta_N = \infty$ are assumed.

On the basis of the above assumptions, we consider the properties of the function $(\mathrm{d}w/\mathrm{d}z)^{\mathrm{i}}$, i being the imaginary unit, the argument of which is the logarithm of the velocity modulus. Thus, moving along an infinitesimal semicircle in the ζ-plane centred at $\zeta = \mathrm{i}\eta_j$, the argument of $(\zeta - \mathrm{i}\eta_j)$ changes by π, while the corresponding change in the argument of $(\mathrm{d}w/\mathrm{d}z)^{\mathrm{i}}$ is $(\ln v_j - \ln v_{j-1})$. Therefore, near $\zeta = \mathrm{i}\eta_j$ we have that

$$\left(\frac{\mathrm{d}w}{\mathrm{d}z}\right)^{\mathrm{i}} \sim (\zeta - \mathrm{i}\eta_j)^{[\ln(v_j/(v_{j-1}))]/\pi}, \quad j = 1{-}N.$$

Similarly, moving along infinitesimal semicircles in the ζ-plane centred at $\zeta = c$ and at $\zeta = a$, the arguments of $(\zeta - c)$ and $(\zeta - a)$ change by π. According to the boundary conditions (2.3), the corresponding changes in the argument of $\mathrm{d}w/\mathrm{d}z$ is $(-\pi + 2\alpha)$ and π for points C and A, respectively. As a result, the local behaviour of $\mathrm{d}w/\mathrm{d}z$ in the ζ-plane is $\mathrm{d}w/\mathrm{d}z \sim (\zeta - c)^{(2\alpha-\pi)/\pi}$ about C and $\mathrm{d}w/\mathrm{d}z \sim (\zeta - a)$ about A. There are no other points in the flow domain where the velocity might be zero or infinity.

With the aim of satisfying the boundary conditions along the solid boundary, that is along the real axis in the ζ-plane, and along the free surface, that is along the imaginary axis, mirror images are considered. Singularities at the inverse order are introduced at each symmetric point, thus giving

$$f(\zeta) = v_N \exp(-\mathrm{i}\pi + \mathrm{i}\beta_L)\left(\frac{\zeta - a}{\zeta + a}\right)\left(\frac{\zeta + c}{\zeta - c}\right)^{1-2\alpha/\pi} \prod_{j=1}^{N}\left(\frac{\zeta - \mathrm{i}\eta_j}{\zeta + \mathrm{i}\eta_j}\right)^{-(\mathrm{i}/\pi)\ln(v_j/(v_{j-1}))}.$$

The argument of $(\eta - \eta_j)$ is defined as

$$\arg(\eta - \eta_j) = \begin{cases} -\pi, & \eta < \eta_j \\ 0, & \eta > \eta_j \end{cases}$$

because when moving in the counterclockwise direction along an infinitesimal semicircle of radius ε in the ζ-plane centred at $\zeta = \mathrm{i}\eta_j$, $\arg(\zeta - \mathrm{i}\eta_j) \to (-\pi)$ as $\zeta \to \mathrm{i}(\eta_j - \varepsilon)$ and $\arg(\zeta - \mathrm{i}\eta_j) \to 0$ as $\zeta \to \mathrm{i}(\eta_j + \varepsilon)$, as shown in figure 1(*b*).

From the definition of $f(\zeta)$, the function $F(\zeta) = (\mathrm{dw}/\mathrm{dz})/f(\zeta)$ contains no singularities in the whole ζ-plane, including the point at infinity, thus implying that $F(\zeta)$ is holomorphic and bounded. According to Liouville's theorem $F(\zeta)$ must be constant. Then, the complex velocity can be written as

$$\frac{\mathrm{d}w}{\mathrm{d}z} = v_N \exp(-\mathrm{i}\pi + \mathrm{i}\beta_L)\left(\frac{\zeta - a}{\zeta + a}\right)\left(\frac{\zeta + c}{\zeta - c}\right)^{1-2\alpha/\pi} \prod_{j=1}^{N}\left(\frac{\zeta - \mathrm{i}\eta_j}{\zeta + \mathrm{i}\eta_j}\right)^{-(\mathrm{i}/\pi)\ln(v_j/(v_{j-1}))},$$

in which the stepwise variation assumed for the velocity modulus along the free surface appears. By taking the limit as the step in the velocity modulus tends to zero and, correspondingly, $N \to \infty$, the last factor in the above equation can be recast in

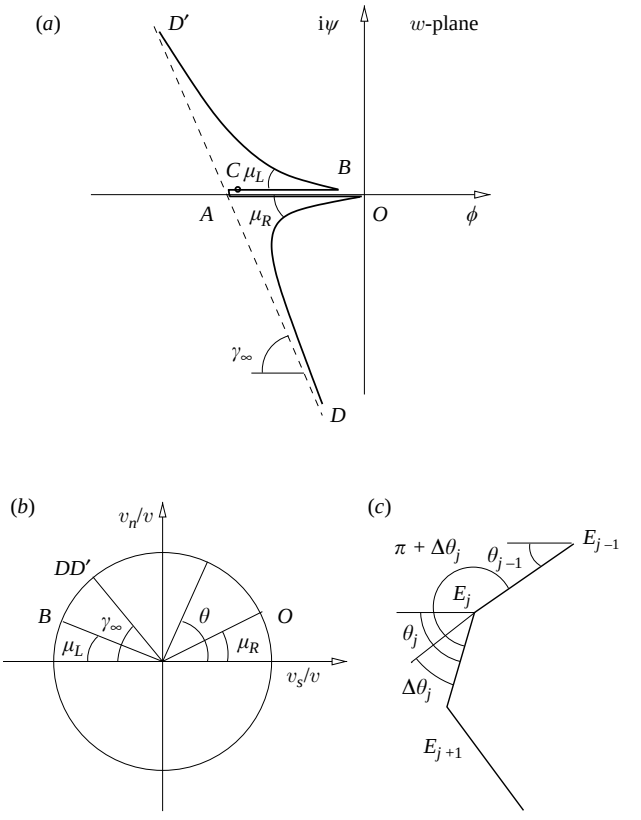

FIGURE 2. Sketches of (*a*) the fluid domain in the w-plane, (*b*) the hodograph of the function θ and (*c*) of the free surface discretization.

exponential form, and letting $\ln(v_j/v_{j-1}) = (\mathrm{d}\ln v/\mathrm{d}\eta)\Delta\eta$ we obtain

$$\frac{\mathrm{d}w}{\mathrm{d}z} = v_B\left(\frac{\zeta-a}{\zeta+a}\right)\left(\frac{\zeta+c}{\zeta-c}\right)^{1-2\alpha/\pi}\exp\left[-\frac{\mathrm{i}}{\pi}\int_0^\infty \frac{\mathrm{d}\ln v}{\mathrm{d}\eta'}\ln\left(\frac{\zeta-\mathrm{i}\eta'}{\zeta+\mathrm{i}\eta'}\right)\mathrm{d}\eta' - \mathrm{i}(\pi-\mathrm{i}\beta_L)\right],$$

which, taking into account that $\arg(\zeta-\mathrm{i}\eta) = \arg(\mathrm{i}\eta-\zeta)-\pi$, finally leads to the continuous form:

$$\frac{\mathrm{d}w}{\mathrm{d}z} = \left(\frac{\zeta-a}{\zeta+a}\right)\left(\frac{\zeta+c}{\zeta-c}\right)^{1-2\alpha/\pi}\exp\left[-\frac{\mathrm{i}}{\pi}\int_0^\infty \frac{\mathrm{d}\ln v}{\mathrm{d}\eta'}\ln\left(\frac{\mathrm{i}\eta'-\zeta}{\mathrm{i}\eta'+\zeta}\right)\mathrm{d}\eta' - \mathrm{i}(\pi-\mathrm{i}\beta_L)\right]. \tag{2.4}$$

It can be easily verified that for $\zeta = \xi$ the argument of equation (2.4) satisfies conditions (2.3) while, for $\zeta = \mathrm{i}\eta$, its modulus is just the function $v(\eta)$.

2.2. *Expression for the derivative of the complex potential*

The complex potential has singularities at the points O, A, B and D which correspond to the corner points of the domain boundary in the w-plane, as shown in figure 2(*a*). Let μ_R and μ_L denote the contact angles at the intersection points on the right- and left-hand side, respectively. Since the velocity has no singularity there, the domain boundary in the w-plane and z-plane has the same angle. Moving along an infinitesimal semicircle with centre at O in the ζ-plane, $\arg(\zeta)$ changes by $\pi/2$,

while the corresponding change in $\arg(w-w_0)$ is μ_R. Hence, the local mapping should behave like $\zeta^{2\mu_R/\pi}$, differentiation of which provides $\mathrm{d}w/\mathrm{d}\zeta \sim \zeta^{2\mu_R/\pi-1}$.

Similarly, moving around a semicircle with centre at D, that is $\zeta=\mathrm{i}$, the argument $\arg(\zeta-\mathrm{i})$ changes by π and the corresponding change in $\arg(w-\infty)$ is $-\pi$. Therefore, the complex potential has a simple pole, that is $w \sim (\zeta-\mathrm{i})^{-1}$ and $\mathrm{d}w/\mathrm{d}z \sim (\zeta-\mathrm{i})^{-2}$. In the same way it is possible to show that near A we have $w \sim (\zeta-a)^2$ and $\mathrm{d}w/\mathrm{d}z \sim (\zeta-a)$.

In order to analyse the behaviour of the velocity potential along the free surface, it is useful to introduce the unit vectors $\boldsymbol{n}$ and $\boldsymbol{\tau}$ denoting the normal and the tangent to the free surface. The normal vector $\boldsymbol{n}$ is directed out from the fluid domain whereas the spatial coordinate along the domain boundary s increases in the direction in which the free surface has the fluid domain to the left (figure 1). With this notation, $\mathrm{d}w = (v_s+\mathrm{i}v_n)\mathrm{d}s$, where v_s and v_n are the tangential and normal velocity components, respectively. Let $\theta(\eta)$ denote the angle between the velocity vector on the free surface and the unit vector $\boldsymbol{\tau}$; it follows that $\theta(\eta) = \tan^{-1}(v_n/v_s)$, the behaviour of which along the free surface is shown in figure 2(*b*).

As already done for the velocity modulus, in a first step we assume that this function is piecewise constant. Once the discrete form is obtained the continuous expression is recovered by taking the limit as the step tends to zero and, correspondingly, the number of elements tends to infinity. We assume that $\theta(\eta) = \theta_j$ on each interval (E_{j-1}, E_j), which is $\eta \in (\eta_{j-1}, \eta_j)$, with a jump $\Delta\theta_{j-1} = \theta_j - \theta_{j-1}$ at $\zeta = \mathrm{i}\eta_{j-1}$ (see figure 2*c*). By taking into account the change in the arguments, it can be shown that the mapping function must behave like $(w - w_j) \sim (\zeta - \mathrm{i}\eta_j)^{1+\Delta\theta_j/\pi}$, from which $\mathrm{d}w/\mathrm{d}\zeta \sim (\zeta - \mathrm{i}\eta_j)^{\Delta\theta_j/\pi}$, $j = 1{-}N$. From the above considerations, we need to construct the function $\mathrm{d}w/\mathrm{d}\zeta$, the argument of which is 0 where $\eta = 0$ and $0 < \xi < \infty$ and is $\theta_j - \pi/2$ where $\xi = 0$ and $\eta_{j-1} < \eta < \eta_j$. Moreover, additional mirror singularities at $\zeta = -a$, $\zeta = -\mathrm{i}$ and $\zeta = -\mathrm{i}\eta_j$, $j = 1{-}N$ must be considered, with the same order of singularity as the corresponding ones in the symmetric positions. By multiplying all the singularities and following the same procedure used before, we finally obtain

$$\frac{\mathrm{d}w}{\mathrm{d}\zeta} = K\zeta^{2\mu_R/\pi-1}\frac{(\zeta^2-a^2)}{(\zeta^2+1)^2}\exp\left(\frac{1}{\pi}\int_0^\pi \frac{\mathrm{d}\theta}{\mathrm{d}\eta'}\ln(\zeta^2+\eta'^2)\mathrm{d}\eta'\right). \tag{2.5}$$

Integration of equation (2.5) in the parameter domain provides the function that conformally maps the parameter domain onto the corresponding domain in the complex potential plane:

$$w(\zeta) = w(0) + \int_0^\zeta K\zeta^{2\mu_R/\pi-1}\frac{(\zeta^2-a^2)}{(\zeta^2+1)^2}\exp\left(\frac{1}{\pi}\int_0^\pi \frac{\mathrm{d}\theta}{\mathrm{d}\eta'}\ln(\zeta^2+\eta'^2)\mathrm{d}\eta'\right)\mathrm{d}\zeta, \tag{2.6}$$

while from the ratio between equation (2.5) and (2.4) we obtain the expression

$$\frac{\mathrm{d}z}{\mathrm{d}\zeta} = K\zeta^{2\mu_R/\pi-1}\frac{(\zeta+a)^2}{(1+\zeta^2)^2}\left(\frac{\zeta-c}{\zeta+c}\right)^{(1-2\alpha/\pi)}\exp\left[\frac{1}{\pi}\int_0^\infty \frac{\mathrm{d}\theta}{\mathrm{d}\eta'}\ln(\eta'^2+\zeta^2)\,\mathrm{d}\eta'\right.$$
$$\left. + \frac{\mathrm{i}}{\pi}\int_0^\infty \frac{\mathrm{d}\ln v}{\mathrm{d}\eta'}\ln\left(\frac{\zeta-\mathrm{i}\eta'}{\zeta+\mathrm{i}\eta'}\right)\mathrm{d}\eta' + \mathrm{i}(\pi-\beta_L)\right], \tag{2.7}$$

integration of which along the imaginary axis in the parameter domain gives the free surface shape in the z-plane. The parameters a, c, K and the functions $v(\eta)$ and $\theta(\eta)$ are determined from the boundary conditions and from physical considerations.

At infinity, the inflow velocity approaches the value $v_\infty \exp(-\mathrm{i}\gamma_\infty)$. Hence, by taking the argument of equation (2.4) when $\zeta = \mathrm{i}$ we obtain the nonlinear condition

$$-\frac{1}{\pi}\int_0^\infty \frac{\mathrm{d}\ln v}{\mathrm{d}\eta'} \ln\left|\frac{\eta'-1}{\eta'+1}\right| \mathrm{d}\eta' + \left(1-\frac{2\alpha}{\pi}\right)\left(2\arctan\frac{1}{c}-\pi\right)+2\arctan\frac{1}{a}+\pi-\delta-\alpha = 0. \tag{2.8}$$

Furthermore, by definition, the wetted length on the right-hand side of the wedge grows like $V_0 t$ and then the length of the segment OC in the stationary plane is unity, that is $|z_O| = 1$, which implies

$$\int_0^c \left|\frac{\mathrm{d}z}{\mathrm{d}\zeta}\right|_{\zeta=\xi} \mathrm{d}\xi = 1. \tag{2.9}$$

Finally, an additional condition is obtained by enforcing that the y-coordinates of the free surface at the infinity on the right- and left-hand sides have be to the same, that is

$$\mathrm{Im}\left(\oint_{\zeta=\mathrm{i}} \frac{\mathrm{d}z}{\mathrm{d}\zeta}\mathrm{d}\zeta\right) = \pi\mathrm{i}\operatorname*{Res}_{\zeta=\mathrm{i}} \frac{\mathrm{d}z}{\mathrm{d}\zeta} = \lim_{\zeta=\mathrm{i}} \frac{\mathrm{d}}{\mathrm{d}\zeta}\left(\frac{\mathrm{d}z}{\mathrm{d}\zeta}(\zeta-\mathrm{i})^2\right) = 0.$$

By calculating the integral through the residue we get

$$\frac{1}{\pi}\int_0^\infty \frac{\mathrm{d}\theta}{\mathrm{d}\eta'}\frac{\mathrm{d}\eta'}{\eta'^2-1} + \frac{a^2}{a^2+1} - \frac{\mu_R}{\pi-1} = 0. \tag{2.10}$$

Equations (2.8)–(2.10) provide the unknown parameters a, c, K once the functions $v(\eta)$ and $\theta(\eta)$ are specified.

2.3. *Dynamic boundary condition*

As the point O lies on the free surface along which the pressure is constant and equal to the atmospheric value P_a, the Cauchy–Lagrange integral written in the physical plane for the point O and for an arbitrary point in the flow field gives

$$\left.\frac{\partial\Phi}{\partial t}\right|_Z + \frac{V^2}{2} + \frac{P}{\varrho} = \left.\frac{\partial\Phi}{\partial t}\right|_{Z_0} + \frac{V_0^2}{2} + \frac{P_a}{\varrho}. \tag{2.11}$$

We consider the fluid boundary as a function $Z(S,t)$ where t denotes time and S is the arc spatial coordinate which takes the value $S=0$ at the contact point O, is positive moving along the wedge surface and negative moving along the free surface toward the right. By using the self-similar variable $s = S/(V_0 t)$, the fluid boundary in the physical plane is given by

$$Z(S,t) = V_0 t z(s),$$

where $z(s)$ is the equation of the fluid boundary in the stationary plane.

On the basis of the above definitions, we express the time derivative of the velocity potential in terms of the derivatives with respect to S and t, that is

$$\left.\frac{\partial W}{\partial t}\right|_Z = \left.\frac{\partial W}{\partial t}\right|_S - \left.\frac{\partial W}{\partial Z}\right|_t \left.\frac{\partial Z}{\partial t}\right|_S = \left.\frac{\partial W}{\partial t}\right|_S - V^2, \tag{2.12}$$

where $V^2 = U\overline{U}$ is the square of the velocity modulus in the physical plane which is $\partial Z/\partial t|_S = U$ from the kinematic condition and $\partial W/\partial Z|_t = \overline{U}$ from the definition of the complex velocity potential. Since

$$W(S,t) = V_0^2 t w\left(\frac{S}{V_0 t}\right) \Rightarrow \left.\frac{\partial W}{\partial t}\right|_S = V_0^2 w(s) - V_0^2 \frac{\mathrm{d}w}{\mathrm{d}s} s$$

equation (2.12) leads to

$$\left.\frac{\partial W}{\partial t}\right|_Z = V_0^2 w(s) - V_0^2 \frac{\mathrm{d}w}{\mathrm{d}s} s - V_0^2 v^2. \tag{2.13}$$

If the complex potential is set to zero at point O, that is $W(Z_0,t) = V_0^2 t w(0) = 0$, where $Z_0 = V_0 t \mathrm{e}^{\mathrm{i}\beta_R}$, by applying equation (2.13) at $s = 0$ it follows that

$$\left.\frac{\partial W}{\partial t}\right|_{Z=V_0 t} = -v^2 V_0^2 = -V_0^2,$$

that is $v^2 = 1$ at O. By using the above result along with the real part of equation (2.12), we finally obtain

$$v^2 = 1 + 2\phi - 2\frac{\mathrm{d}\phi}{\mathrm{d}s} s, \tag{2.14}$$

which is valid at any point lying on the free surface.

By taking the derivative of equation (2.14) with respect to s and accounting for the relations $\mathrm{d}\phi/\mathrm{d}s = v_s$ and $v_s = v\cos\theta$, the following differential equation is obtained:

$$\frac{\mathrm{d}\ln v}{\mathrm{d}s} = \frac{s\sin\theta}{v + s\cos\theta}\frac{\mathrm{d}\theta}{\mathrm{d}s}, \tag{2.15}$$

which shows the relation between the derivative of the modulus and the derivative of the angle of the velocity at the free surface. It is worth noting that the above equation is derived using only the self-similarity and therefore it holds along the free boundary of any two-dimensional self-similar problem.

By multiplying both sides of equation (2.15) by $\mathrm{d}s/\mathrm{d}\eta$, we obtain

$$\frac{\mathrm{d}\ln v}{\mathrm{d}\eta} = \frac{s\sin\theta}{v + s\cos\theta}\frac{\mathrm{d}\theta}{\mathrm{d}\eta}, \tag{2.16}$$

where

$$s(\eta) = -\int_0^\eta \left|\frac{\mathrm{d}z}{\mathrm{d}\zeta}\right|_{\zeta=i\eta} \mathrm{d}\eta = -K\int_0^\eta \frac{\eta^{2\mu_R/\pi-1}}{v(\eta)}\frac{\eta^2 + a^2}{(1-\eta^2)^2}\exp\left[\frac{1}{\pi}\int_0^\infty \frac{\mathrm{d}\theta}{\mathrm{d}\eta'}\ln\left|\eta'^2 - \eta^2\right|\mathrm{d}\eta'\right]\mathrm{d}\eta. \tag{2.17}$$

The set of equations (2.14)–(2.17) is valid for the right-hand side only. A similar set can be derived for the left-hand side by assuming $W(Z_B,t) = 0$.

2.4. *Kinematic boundary condition*

Since the pressure is constant along the free surface the acceleration of the fluid particles is orthogonal to the boundary

$$\mathrm{Re}\left(\frac{\partial U}{\partial t}\overline{\mathrm{d}Z}\right) = 0. \tag{2.18}$$

Let γ denote the argument of the velocity vector U and χ the argument of a small element $\mathrm{d}Z$ lying on the free surface. Thus, by using the similarity relations to pass

from the variables in the physical plane to the corresponding ones in the stationary plane, we obtain

$$\left.\frac{\partial U}{\partial t}\right|_S = V_0\frac{\mathrm{d}u}{\mathrm{d}s}\left(-\frac{s}{t}\right) = V_0\frac{\mathrm{d}u}{\mathrm{d}\eta}\frac{\mathrm{d}\eta}{\mathrm{d}s}\left(-\frac{s}{t}\right), \qquad \mathrm{d}Z = V_0^2 t\left(\frac{\mathrm{d}w}{\mathrm{d}\zeta}\Big/\frac{\mathrm{d}w}{\mathrm{d}z}\right)\mathrm{d}\zeta = V_0^2 t\mathrm{e}^{\mathrm{i}\chi}\mathrm{d}s,$$

where $u = v\mathrm{e}^{\mathrm{i}\gamma}$. In the above equation the derivative of u with respect to η is

$$\frac{\mathrm{d}u}{\mathrm{d}\eta} = v\mathrm{e}^{\mathrm{i}\gamma}\left(\frac{\mathrm{d}\ln v}{\mathrm{d}\eta} + \mathrm{i}\frac{\mathrm{d}\gamma}{\mathrm{d}\eta}\right),$$

use of which in the condition (2.18) leads to

$$\frac{\mathrm{d}\gamma}{\mathrm{d}\eta} = -\frac{1}{\tan\theta}\frac{\mathrm{d}\ln v}{\mathrm{d}\eta}, \tag{2.19}$$

where, by definition, $\theta = \chi - \gamma$.

By writing equation (2.4) for $\zeta = \mathrm{i}\eta$, another equation for γ can be obtained as

$$\gamma = \mathrm{Im}\left(\ln\overline{\frac{\mathrm{d}w}{\mathrm{d}z}}\right)$$

the derivative of which with respect to η provides

$$\frac{\mathrm{d}\gamma}{\mathrm{d}\eta} = \frac{2a}{\eta^2 + a^2} + \left(\frac{2\alpha}{\pi} - 1\right)\frac{2c}{\eta^2 + c^2} - \frac{1}{\pi}\int_0^\infty \frac{\mathrm{d}\ln v}{\mathrm{d}\eta'}\frac{2\eta'}{\eta'^2 - \eta^2}\,\mathrm{d}\eta'. \tag{2.20}$$

From equations (2.19) and (2.20), the following integral equation in terms of $\mathrm{d}\ln v/\mathrm{d}\eta$ is obtained:

$$-\frac{1}{2\tan\theta}\frac{\mathrm{d}\ln v}{\mathrm{d}\eta} + \frac{1}{\pi}\int_0^\infty \frac{\mathrm{d}\ln v}{\mathrm{d}\eta'}\frac{\eta'}{\eta'^2 - \eta^2}\mathrm{d}\eta' = \frac{a}{\eta^2 + a^2} + \left(\frac{2\alpha}{\pi} - 1\right)\frac{c}{\eta^2 + c^2}. \tag{2.21}$$

The system of equation (2.8)–(2.10), (2.16), (2.21) is closed and determines the parameters a, c, K and the unknown functions $v(\eta)$ and $\theta(\eta)$.

On the wedge sides, the normal velocity component is zero so that $\theta_R = \pi$ and $\theta_L = 0$, with θ_R and θ_L denoting the angle that the velocity forms with respect to the tangent vector $\boldsymbol{\tau}$ along the body (see figure 1*a*). Once the function $\theta(\eta)$ is evaluated, the contact angles between the wedge sides and the free surface, μ_R and μ_L, can be determined as follows (see figure 2*b*):

$$\mu_R = \theta_R - \Big[\pi - \lim_{\eta\to 0}\theta(\eta)\Big] = \theta(0), \qquad \mu_L = \Big[\pi - \lim_{\eta\to\infty}\theta(\eta)\Big] - \theta_L = \pi - \lim_{\eta\to\infty}\theta(\eta). \tag{2.22}$$

2.5. *Pressure distribution*

In order to evaluate the pressure distribution on the solid surface, the term $\partial\Phi/\partial t$ in equation (2.11) has to be written in terms of the quantities in the stationary plane z. In the physical plane the wedge surface is given by the following expressions:

$$Z(S,t) = V_0 t\left(1 - \frac{S}{V_0 t}\right)\mathrm{e}^{\mathrm{i}\beta_R}, \qquad 0 \leqslant S \leqslant V_0 t,$$

$$Z(S,t) = V_0 t\left(\frac{S}{V_0 t} - 1\right)\mathrm{e}^{\mathrm{i}(\pi-\beta_L)}, \qquad V_0 t \leqslant S \leqslant (V_0 + V_B)t,$$

for the right- and left-hand sides, respectively, from which it follows that

$$\left.\frac{\partial Z}{\partial t}\right|_S = V_0 e^{i\beta_R}, \qquad 0 \leqslant S \leqslant V_0 t,$$
$$\left.\frac{\partial Z}{\partial t}\right|_S = -V_0 e^{i(\pi-\beta_L)}, \qquad V_0 t \leqslant S \leqslant (V_0 + V_B)t.$$

By substituting the above expressions into equation (2.12) and taking into account that the imaginary part of the complex potential equals zero on the solid surface, we obtain

$$\left.\frac{\partial \Phi}{\partial t}\right|_Z = \left.\frac{\partial \Phi}{\partial t}\right|_S - vV_0^2 = V_0^2\phi + V_0^2 v(s-1), \quad 0 \leqslant s \leqslant 1,$$
$$\left.\frac{\partial \Phi}{\partial t}\right|_Z = \left.\frac{\partial \Phi}{\partial t}\right|_S + vV_0^2 = V_0^2\phi + V_0^2 v(1-s), \quad 1 \leqslant s \leqslant 1 + v_B.$$

By using the above results in equation (2.11) the following expressions for the pressure coefficient $p = 2P/(\varrho V_\infty^2)$ are finally recovered:

$$p_R(\xi) = -\frac{2(\phi + sv) + (1-v)^2}{v_\infty^2}, \quad 0 \leqslant \xi \leqslant c, \tag{2.23}$$

$$p_L(\xi) = -\frac{2(\phi - sv) + (1+v)^2}{v_\infty^2}, \quad c \leqslant \xi \leqslant \infty, \tag{2.24}$$

where ϕ, v, s are determined from equation (2.6), (2.4) and (2.7) as

$$\phi = \mathrm{Re}(w(\zeta)|_{\zeta=\xi}), \qquad v = \left|\frac{\mathrm{d}w}{\mathrm{d}z}\right|_{\zeta=\xi}, \qquad s(\xi) = \int_0^\xi \left|\frac{\mathrm{d}z}{\mathrm{d}\zeta}\right|_{\zeta=\xi} \mathrm{d}\xi.$$

3. Numerical method and validation

3.1. *Numerical approach*

The boundary value problem under consideration is reduced to a system of nonlinear equations including the integro-differential equation (2.16) and integral equation (2.21). It is possible to eliminate the function $\mathrm{d}\ln v/\mathrm{d}\eta$ by using equation (2.16) and reduce the problem to one singular integral equation similar to that obtained by Dobrovol'skaya (1969). However, it is much easier to derive the solution of the system through the method of successive approximations. The method consists of applying the Hilbert transform to solve the equation (2.21) and determining the $(k+1)$th approximation as follows:

$$\left(\frac{\mathrm{d}\ln v}{\mathrm{d}\eta}\right)^{k+1} = \frac{4}{\pi}\int_0^\infty \left\{\frac{1}{2\tan\theta}\frac{\mathrm{d}\ln v}{\mathrm{d}\eta'} + \frac{a}{a^2+\eta'^2} + \left(\frac{2\alpha}{\pi} - 1\right)\frac{c}{c^2+\eta'^2}\right\}^k \frac{\eta'}{\eta'^2-\eta^2}\,\mathrm{d}\eta'. \tag{3.1}$$

From equation (2.21) we find the $(k+1)$th approximation of the derivative $\mathrm{d}\theta/\mathrm{d}\eta$

$$\left(\frac{\mathrm{d}\theta}{\mathrm{d}\eta}\right)^{k+1} = \frac{v^{k+1} + s^k\cos\theta^k}{s^k\sin\theta^k}\left(\frac{\mathrm{d}\ln v}{\mathrm{d}\eta}\right)^{k+1}, \tag{3.2}$$

integration of which along the imaginary axis of the parameter domain provides the $(k+1)$th approximation for the function $\theta(\eta)$. The system of nonlinear equations

(2.8)–(2.10) is solved at each iteration. The functions $\mathrm{d}\ln v/\mathrm{d}\eta$ and $\mathrm{d}\theta/\mathrm{d}\eta$ are defined for any $0 < \eta < \infty$ and, correspondingly, for any free surface point.

In discrete form the solution is enforced at a fixed set of points η_j , $j = 1$–N lying on the imaginary axis of the parameter domain. The functions $v(\eta)$ and $\theta(\eta)$ are interpolated linearly on intervals (η_{j-1}, η_j) to obtain analytical expressions for the integrals in (2.4) and (2.5), thus allowing a reduction of the computational effort. The first point $\eta_1 = \varepsilon$ and the last one η_N are chosen enough small and enough large, respectively, to achieve good accuracy. The arclength s_1 of the free surface point nearest to O is analytically evaluated by taking into account the singularity in the integrand of equation (2.17), thus obtaining

$$s_1 = -Ka^2 \exp\left(\frac{2}{\pi}\int_0^\infty \frac{\mathrm{d}\theta}{\mathrm{d}\eta'}\ln\eta'\mathrm{d}\eta'\right)\frac{\eta_1^{2\mu_R/\pi}}{2\mu_R/\pi}. \tag{3.3}$$

In a similar way, to derive the arclength s_N of the point nearest to B, the integral in equation (2.17) for $\eta \gg \eta_N$ is written as

$$\frac{1}{\pi}\int_0^\infty \frac{\mathrm{d}\theta}{\mathrm{d}\eta'}\ln|\eta'^2 - \eta^2|\mathrm{d}\eta' = \frac{2\ln\eta}{\pi}(\theta(\infty) - \theta(0)) = \frac{2\ln\eta}{\pi}(\pi - \mu_R - \mu_L)$$

which provides

$$s_N = \frac{K}{v_B}\frac{\eta_N^{-2\mu_L/\pi}}{2\mu_L/\pi}. \tag{3.4}$$

Equations (3.3) and (3.4) show that, if the contact angle $\mu_R \to 0$ ($\mu_L \to 0$), the arclength s_1 (s_N) of the free surface point nearest to O (B), which mean the jet length, tends to infinity as $1/\mu_R$ ($1/\mu_L$).

3.2. *Validation for the symmetric wedge impact*

For validation purposes, the numerical approach is applied to derive the similarity solution of the flow about symmetric wedges impacting the free surface. With the aim of evaluating the accuracy and grid-independence of the results, two different distributions of the nodes η_j have been generated and employed in deriving the solution. A first set of points is chosen to be symmetric with respect to $\eta = 1$ and distributed as a geometric series in the interval $0 < \eta_j < 1$, for $j = 1$–$N/2$, with $\eta_1 = 10^{-5}$, and $\eta_j = 1/\eta_{N-j}$, for $j = N/2+1$–N. This symmetric distribution of nodes in the parameter domain corresponds to an almost symmetric distribution (within 3%) of the nodes along the free surface in the physical plane. The numerical results approach the solution of the integral equation (2.21) as $\eta_1 \to 0$ and $N \to \infty$. However, too small values of the ratio η_1/η_N (say $\eta_1/\eta_N < 10^{-10}$) make the achievement of good results using only fifteen figures in the number representation difficult. In order to improve the accuracy, at least on the right-hand side, an asymmetric distribution is used instead. The integration domain is divided into six parts, and within each part $N/6$ nodes are distributed as a geometric series. The first element has been set to $\eta_1 = 5 \times 10^{-7}$, while the last elements of each part are: $\eta_{N/6} = 0.002$, $\eta_{N/3} = 0.1$, $\eta_{N/2} = 1$, $\eta_{2N/3} = 1/\eta_{N/3}$, $\eta_{5N/6} = 1/\eta_{N/6}$ and $\eta_N = 5 \times 10^3$. Calculations are usually carried out using $N = 420$.

The derivation of the solution about the jet tips is usually very challenging. In particular, as discussed by Dobrovol'skaya (1969), the contact angle at the intersection is a basic parameter and a good estimate of it is essential to get good accuracy

α (deg.)	Zhao & Faltinsen	Symmetric distribution		Asymmetric distribution	
	μ/π	μ_R/π	μ_L/π	μ_R/π	μ_L/π
9	0.07153	0.07247	0.07217	0.07162	0.07785
20	0.04992	0.05028	0.05018	0.04996	0.05236
30	0.03591	0.03613	0.03606	0.03594	0.03728
40	0.02514	0.02529	0.02523	0.02515	0.02601
50	0.01663	0.01675	0.01670	0.01664	0.01722
60	0.009913	0.010000	0.009962	0.009916	0.010364
70	0.004783	0.004860	0.004829	0.004790	0.005168
80	0.001337	0.001388	0.001369	0.001345	0.001560

TABLE 1. Contact angles obtained for the impact of symmetric wedges having different angles α. Results obtained on the left- and right-hand side by using the symmetric and asymmetric distributions of the nodes are compared with those obtained by Zhao & Faltinsen (1993).

throughout the fluid domain. In table 1, the contact angles predicted by the present method are compared with the corresponding ones obtained through Dobrovol'skaya's model by Zhao & Faltinsen (1993). Similar results in terms of contact angles have been also obtained by Keady & Fowkes (1998). It is worth remarking that the results by Zhao & Faltinsen (1993) were obtained using 10^{-25} as the smallest integration step when solving Dobrovol'skaya's integral equation.

In table 1, results obtained by the present approach are listed in terms of the left and right contact angles in order to show the intrinsic asymmetry of the numerical method. From the results it can be seen that the symmetric distributions with $\eta_1 = 10^{-5}$ provide accuracy of calculations in the range $(0.6-4)\%$ for both left and right contact angles, while, by using the asymmetric distribution with $\eta_1 = 5 \times 10^{-7}$, we achieve a much better accuracy for the right-hand side, $(0.04 - 0.6)\%$, and a worse accuracy for the left, (3–8) %.

The difference between the results corresponding to symmetric and asymmetric distributions is caused by the location of the first ($\eta_1 = \varepsilon$) and last (η_N) points on the imaginary axis. If η_1 decreases, i.e. the corresponding arclength s_1 decreases as follows from equation (3.3), the contact angle at the right-hand side approaches the Zhao & Faltinsen (1993) results. On the contrary, if η_N decreases, the corresponding arclength s_N increases as follows from equation (3.4) and the accuracy of the predicted contact angle at the left-hand side decreases. However, the reduced accuracy of the prediction of the flow at the jet tip on the left-hand side does not affect the accuracy on the other side. This led us to exploit the mirror symmetry in the asymmetric wedge computations: for each case the solutions for positive and negative heel angles are calculated, thus achieving an accurate prediction of the flow parameters on both wedge sides without the need of using more than fifteen figures in the number representation.

With the aim of evaluating the effect of the number of nodes, in table 2 a comparison is presented, in terms of the angle at the intersection and of the maximum pressure coefficient p_{max}, among results obtained by using $N = 420$ and $N = 840$ and those reported in Zhao & Faltinsen (1993). As the asymmetric distribution of nodes is used, the data from the right-hand side are listed in the table, being the most accurate. The comparison indicates that convergence is achieved as the number of nodes is increased although the variation is less than 1%.

α (deg.)	μ/π (ZF)	μ_R/π ($N = 420$)	μ_R/π ($N = 840$)	p_{max} (ZF)	p_{max} ($N = 420$)	p_{max} ($N = 840$)
60	0.009913	0.009916	0.009902	6.927	6.888	6.894
70	0.004783	0.004796	0.004782	17.774	17.702	17.735
80	0.001337	0.001355	0.001345	77.847	77.112	77.544

TABLE 2. Effect of the number of nodes on the angle at the intersection and on the maximum pressure coefficient for different wedge angles α. Results by the present method are shown in terms of the right-hand-side quantities which are the most accurate when using the asymmetric distribution of nodes. The corresponding quantities reported in Zhao & Faltinsen (1993) (ZF) are also shown.

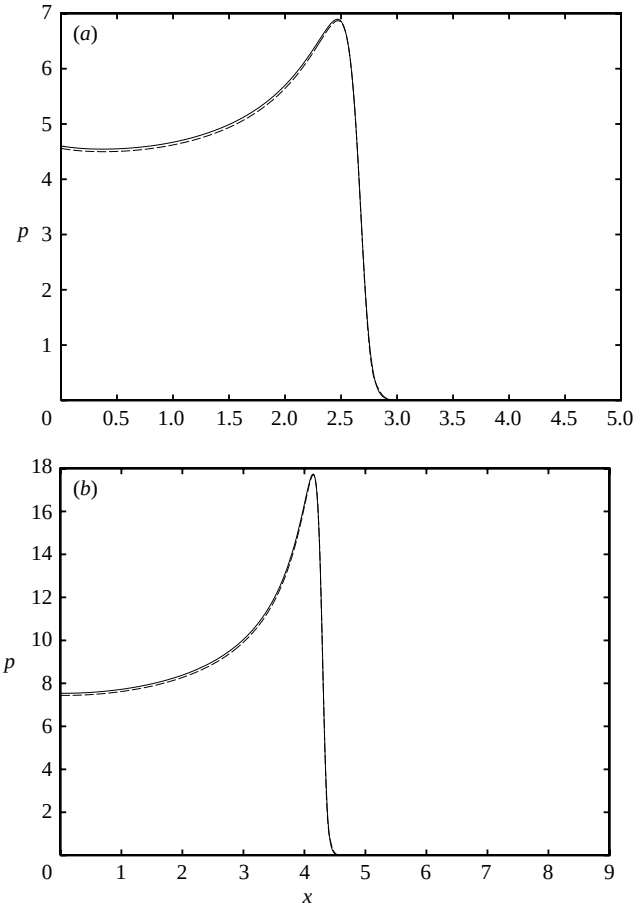

FIGURE 3. Pressure coefficient versus the horizontal coordinate x for (a) $\alpha = 60^\circ$ and (b) $\alpha = 70^\circ$. Results by the present model (solid) are compared with those obtained through the self-similar model described in Battistin & Iafrati (2004) (dashed).

As a further validation of the model, in figure 3 a comparison is shown in terms of the pressure coefficients obtained by the present approach and by the self-similar model proposed in Battistin & Iafrati (2004). The comparison, established for two different wedge angles, exhibits a good agreement throughout the wetted body contour.

δ (deg.)	μ_R/π	μ'_L/π	y_O	y'_B	$p_{R\,max}$	$p'_{L\,max}$
0	0.009916	0.009913*	1.834	1.836*	6.888	6.927*
5	0.013851	0.006778	1.852	1.822	5.072	9.958
10	0.018778	0.004307	1.886	1.809	3.968	15.61
15	0.025035	0.002425	1.956	1.792	3.757	27.72
20	0.033197	0.001097	2.112	1.761	3.579	61.25

TABLE 3. Effect of the heel angle δ on the angle at the intersections and on the maximum pressure coefficient for a wedge with $\alpha = 60°$. Quantities marked * denotes data reported in Zhao & Faltinsen (1993) for the corresponding symmetric wedge case.

4. Asymmetric wedge impact

4.1. *Effect of the heel angle on the solution*

The role played by the asymmetry is investigated by performing numerical calculations for fixed wedge angles and different heel angles δ. Attention is focused on the vertical water entry case, that is $\gamma_\infty = \pi/2$, thus implying that there is no asymmetry due to the horizontal velocity component. As a verification of the numerical approach, the flow about asymmetric wedges has been computed by using the symmetric distribution of the nodes for both a positive and negative heel angle. Differences among the most relevant parameters of the flow have been found to be within 1.5%. With the aim of achieving a higher accuracy, the asymmetric point distribution is employed instead. As the right-hand side is the most accurate when using an asymmetric distribution of nodes, in the following the solution on the left-hand side is taken as that obtained on the right-hand side for negative heel angle, i.e. $\mu'_L(\delta) = \mu_R(-\delta)$. On the basis of the verification carried out for symmetric wedges, reported in tables 1 and 2, we expect the same accuracy be achieved for the asymmetric wedge impact.

In table 3 the solutions obtained for a wedge with $\alpha = 60°$ and different heel angles are reported in terms of the contact angles, the free boundary elevation at the intersection points and the pressure peaks on the right- and left-hand sides of the wedge. From the results listed in table 3 it can be seen that, as the wedge rotates in the counterclockwise direction, the angle at the intersection and the maximum free surface elevation on the left-hand side decrease while those on the right-hand side grow. Correspondingly, the pressure peak exhibits a significant growth on the left and a reduction on the right side of the wedge. This behaviour is consistent with the increase of the deadrise angle on the right side, $\beta_R = \pi/2 - \alpha + \delta$, and the reduction of that on the left side, $\beta_L = \pi/2 - \alpha - \delta$.

Graphically, the effect of the asymmetry on the contact angle at the intersection points for wedges with $\alpha = 60°$ and $30°$, is shown in figure 4 where the contact angles are plotted versus the deadrise angle and compared with the solution obtained for the symmetric wedge impact. In both cases, as the wedge rotates, the contact angle is larger on the side with the larger deadrise angle and smaller on the opposite side. Furthermore, for a given δ, the difference with respect to the symmetric solution is larger on the side with the larger deadrise angle. It is also worth noting that, by extrapolating the curve $\mu_R = \mu_R(\beta_R)$ to $\beta_R/\pi = 0.472$ (which is $\beta_R = 85°$), it can be seen that the contact angle on the right-hand side grows beyond the limit value $\mu/\pi = 0.1$ found for the symmetric wedges (Fraenkel & Keady 2004).

The changes induced by the heel angle on the free surface shape are shown in figure 5 where the solution for a wedge with $\alpha = 30°$ rotated by a heel angle $\delta = 15°$

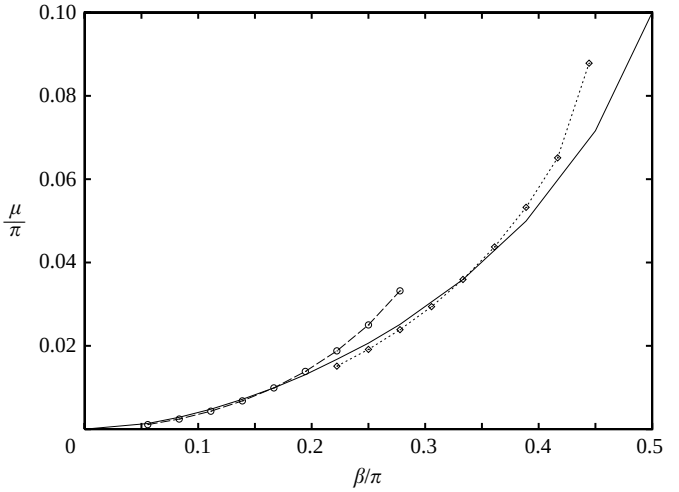

FIGURE 4. Contact angle μ as a function of the deadrise angle for asymmetric wedge impact. Calculations are performed for wedges with $\alpha = 30^\circ$ (dashed, $\diamond$) and 60° (dotted, $\circ$) rotated by a heel angle $\delta = 0, 5^\circ, 10^\circ, 15^\circ, 20^\circ$. For each orientation of the wedge, the left and right contact angles are reported corresponding to the deadrise angle on the left- and right-hand side, respectively. The solid line represents the solution for the symmetric wedge case.

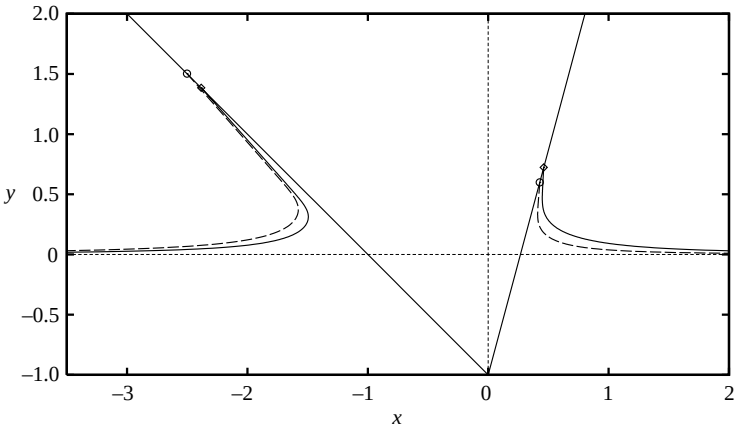

FIGURE 5. Free surface profiles for a wedge with $\alpha = 30^\circ$ impacting with a heel angle $\delta = 15^\circ$. The corresponding symmetric solutions obtained for $\beta = 45^\circ$ and $\beta = 75^\circ$ are shown with dashed lines on the left- and right-hand sides, respectively. The symbols on the two sides represent the contact points for the symmetric ($\circ$) and asymmetric ($\diamond$) cases.

is compared with the free surface shapes of the corresponding symmetric solutions. From this figure, we can see how the higher pressure field on the side with the smaller deadrise angle forces the fluid to move toward the other side. Hence, as discussed above, the free surface elevation is reduced on the side with the smaller deadrise angle and increased on the opposite side. Correspondingly, the jet root on the left is closer to the wedge apex while that on the right-hand side moves away from it.

The asymmetry due to the heel angle is also responsible for a rather remarkable change in the pressure distribution. This effect is shown in figure 6 where the pressure distributions obtained for wedges with $\alpha = 30^\circ$ and 60° and heel angles of $\delta = 10^\circ$ and

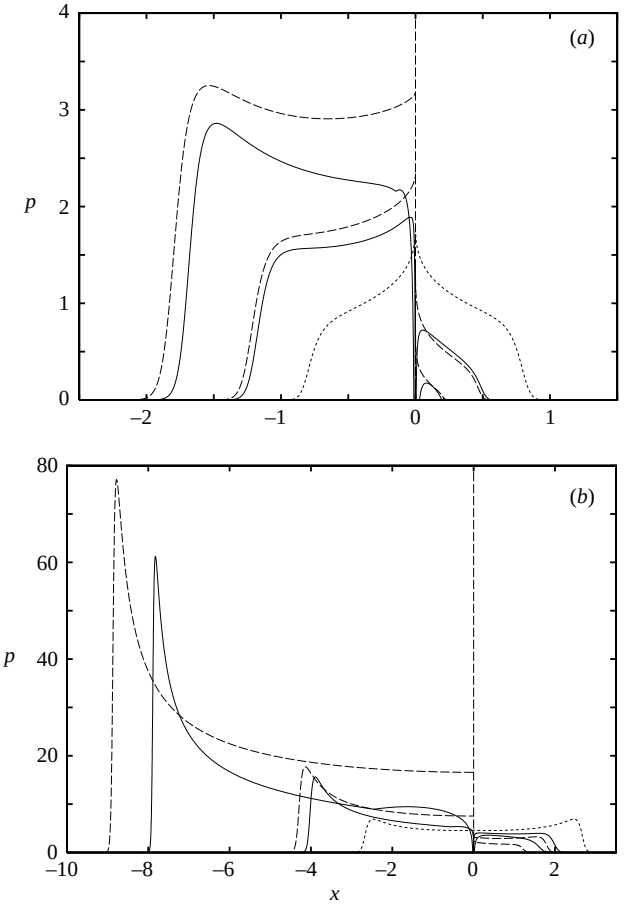

FIGURE 6. Effect of the heel angle on the pressure distributions for wedge angles (*a*) $\alpha = 30^\circ$ and (*b*) $\alpha = 60^\circ$. Results for $\delta = 10^\circ$ and $\delta = 20^\circ$ (solid) are compared with those for $\delta = 0$ (dotted) and with the corresponding symmetric solutions (dashed).

20° are compared with the solution obtained for $\delta = 0$ (at the same wedge angle) and with the corresponding solutions for symmetric wedge impact. As a consequence of the crossflow at the wedge apex, a flow singularity occurs leading to negative pressure in a very small region about $x = 0$, which is not shown in the figures. Moreover, owing to the rotation of the wedge, the pressure on the left-hand side grows and eventually a pressure peak appears although, compared to the symmetric solution, it is much weaker and closer to the wedge apex. On the contrary, on the right-hand side, the pressure is higher and acts on a wider region compared to the corresponding symmetric solutions.

A careful look at the pressure distributions shown in figure 6 for $\delta = 20^\circ$ also reveals a particular behaviour about $x \simeq -0.2$ for $\alpha = 30^\circ$ and $x \simeq -2.5$ for $\alpha = 60^\circ$. In order to investigate this point further, an enlarged view of the distributions of pressure and velocity potential is shown in figure 7(*a*) for the case $\alpha = 60^\circ$ and $\delta = 20^\circ$. The figure indicates that a local minimum in the pressure field occurs at the point where the tangential velocity component $v_s = \mathrm{d}\phi/\mathrm{d}s$ vanishes, which is at the stagnation point in the frame of reference attached to the body. Furthermore, the pressure distribution is characterized by a jump in the tangential derivative which is

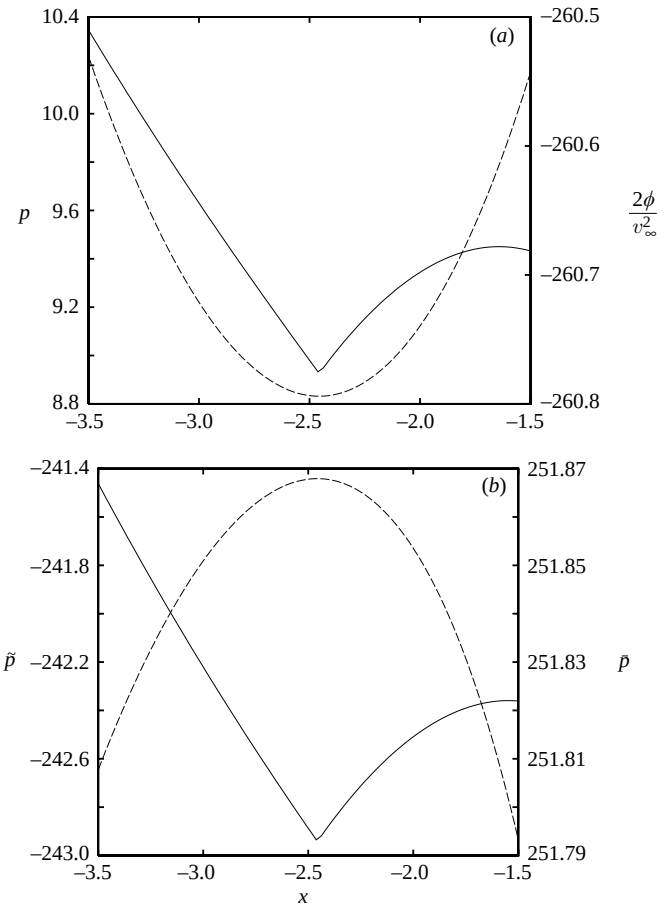

FIGURE 7. Close-up views of the distributions of the pressure p, velocity potential ϕ and the steady $\bar{p}$ and unsteady $\tilde{p}$ pressure components about $x = -2.5$ for a wedge with $\alpha = 60^\circ$ rotated by $\delta = 20^\circ$. According to equations (2.23) and (2.24), in order to make the different terms comparable, the velocity potential ϕ is multiplyed by $2/v_\infty^2$. The graph in (a) indicates that a local minimun of the pressure occurs at the stagnation point where a minimum of the velocity potential occurs. The jump in the tangential derivative of the pressure is directly related to the unsteady component.

related to the behaviour of the velocity modulus about the stagnation point. With the aim of explaining the behaviour of the pressure, let us assume the stagnation point to be located on the right-hand side of the wedge at $s = s^*$ with $s^* < 1$. The pressure p_R can be split into the steady $\bar{p}_R$ and unsteady components $\tilde{p}_R$ for which we have

$$\bar{p}_R = \frac{(1 - v^2)}{v_\infty^2}, \qquad \tilde{p}_R = -\frac{2\,(\phi + vs - v + 1)}{v_\infty^2},$$

differentiation of which with respect to the arclength s yields

$$\frac{\mathrm{d}\bar{p}_R}{\mathrm{d}s} = -\frac{2v}{v_\infty^2}\frac{\mathrm{d}v}{\mathrm{d}s}, \qquad \frac{\mathrm{d}\tilde{p}_R}{\mathrm{d}s} = -\frac{2}{v_\infty^2}\left(\frac{\mathrm{d}\phi}{\mathrm{d}s} + (s-1)\frac{\mathrm{d}v}{\mathrm{d}s} + v\right).$$

At the stagnation point both the velocity modulus and the tangential derivative of the velocity potential vanishes, i.e. $v = 0$ and $\mathrm{d}\phi/\mathrm{d}s = 0$. By analysing the behaviour of

the derivatives $\mathrm{d}v/\mathrm{d}\xi$, $\mathrm{d}s/\mathrm{d}\xi$, it can be shown that about the stagnation point $\xi = a$ the quantity $\mathrm{d}v/\mathrm{d}s = (\mathrm{d}v/\mathrm{d}\xi)/(\mathrm{d}s/\mathrm{d}\xi)$ is finite and different from zero thus providing

$$\frac{\mathrm{d}\bar{p}_R}{\mathrm{d}s} = 0, \qquad \frac{\mathrm{d}\tilde{p}_R}{\mathrm{d}s} = \frac{2(1-s^*)}{v_\infty^2}\frac{\mathrm{d}v}{\mathrm{d}s}.$$

The above equations indicate that the unsteady component is responsible for the jump in the tangential derivative of the pressure, and that the jump is induced by the change in the sign of the derivative of the velocity modulus $\mathrm{d}v/\mathrm{d}s$ about the stagnation point. This is clearly displayed in figure 7(*b*) where the steady and unsteady components of the pressure are plotted separately.

The occurrence of a stagnation point in the frame of reference attached to the impacting wedge is also shown by the streamfunction behaviour. In figure 8, the streamline pattern is shown for four asymmetric conditions. In addition to the stagnation point on the side with the smaller deadrise angle, the figure clearly highlights the crossflow taking place at the apex as a consequence of the flow asymmetry. As stated above, this crossflow is responsible for the pressure and velocity singularities occurring at that point.

In figure 9, results obtained by the present method are compared with those provided by a fully nonlinear numerical approach (Iafrati 2000) for a wedge with $\alpha = 65^\circ$ rotated by a heel angle $\delta = 5^\circ$. The comparison is quite good although small differences occur about the jet regions, probably because in the numerical model the thinnest part of the jet is cut off the computational domain and replaced by a suitable boundary condition enforced at the jet truncation.

4.2. *Force and moment coefficients*

The non-dimensional coefficients of the normal force acting on the right and left wedge sides, C_{nR} and C_{nL}, and the coefficients C_D and C_m of the total vertical force and moment about the wedge apex are evaluated by integrating the pressure along the real axis of the parameter domain:

$$C_{\{nR,nL\}} = \frac{1}{0.5\varrho V_\infty^2 H}\int_0^{V_{\{O,B\}}t} P_{\{R,L\}}(S)\,\mathrm{d}S = \frac{1}{h}\int_{0,c}^{c,\infty} p_{\{R,L\}}[s(\xi)]\frac{\mathrm{d}s}{\mathrm{d}\xi}\mathrm{d}\xi,$$

$$C_D = C_{nR}\sin(\alpha-\delta) + C_{nL}\sin(\alpha+\delta),$$

$$C_m = \frac{1}{h^2}\left\{(1-s(\xi))\frac{\mathrm{d}s}{\mathrm{d}\xi}\right\}\left(\int_0^c p_R[s(\xi)]\mathrm{d}\xi + \int_c^\infty p_L[s(\xi)]\mathrm{d}\xi\right),$$

where

$$s(\xi) = \int_0^\xi \left|\frac{\mathrm{d}z}{\mathrm{d}\zeta}\right|_{\zeta=\xi}\mathrm{d}\xi,$$

and H is the characteristic length in the physical plane which is given by

$$H = V_\infty t h, \quad h = v_\infty(\tan(\alpha-\delta) + \tan(\alpha+\delta)).$$

The integrals in the above expressions converge since the integrand at $\xi = c$, corresponding to the wedge apex, has a singularity $(\xi - c)^{-1+2\alpha/\pi}$ as follows from equations (2.4), (2.7), (2.23) and (2.24).

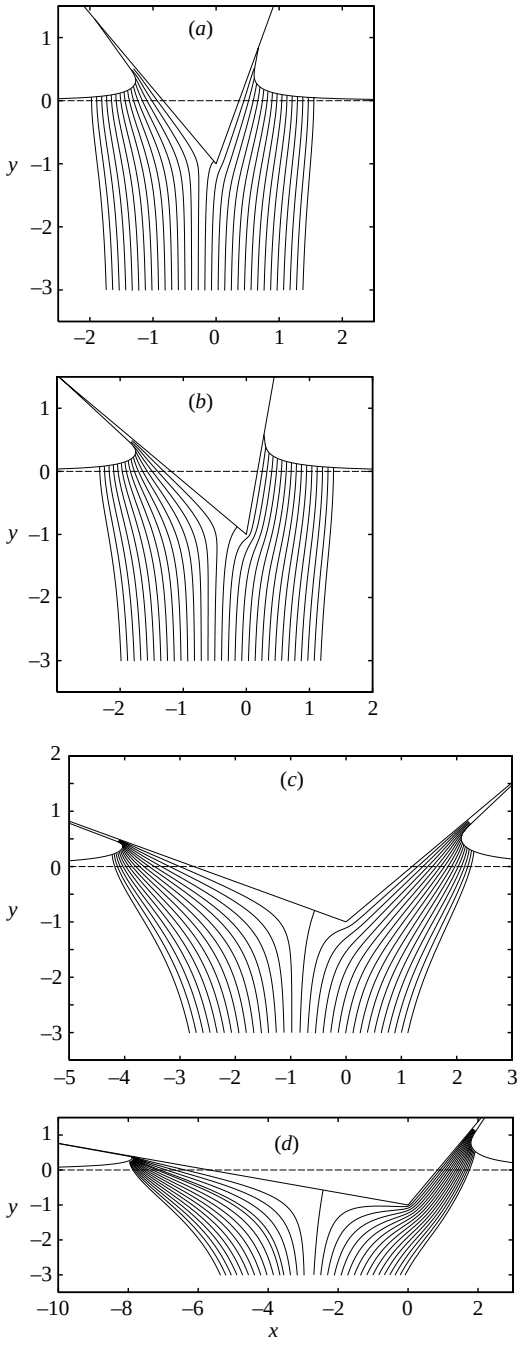

FIGURE 8. Streamline pattern for the asymmetric impact. The occurrence of a stagnation point on the less inclined side of the wedge is clearly evident. (*a*) $\alpha = 30^\circ$, $\delta = 10^\circ$; (*b*) $\alpha = 30^\circ$, $\delta = 20^\circ$; (*c*) $\alpha = 60^\circ$, $\delta = 10^\circ$; (*d*) $\alpha = 60^\circ$, $\delta = 20^\circ$.

In figure 10, the dependence of the force coefficients on δ are presented for $\alpha = 30^\circ$ and 60°. For small δ, the force coefficients vary about linearly with the heel angle, decreasing on the right-hand side and increasing on the left, while the total force

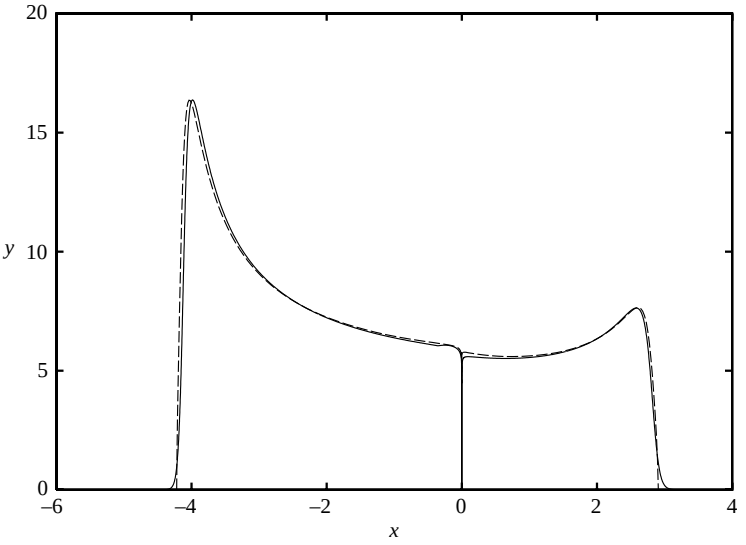

FIGURE 9. Comparison between the pressure distribution obtained by the present approach (solid) and that provided by a fully nonlinear numerical solver (dashed), for a wedge with $\alpha = 65^\circ$ rotated by $\delta = 5^\circ$.

coefficient C_D remains nearly constant. As expected, the drag force takes its minimum for $\delta = 0$, that is for the symmetric wedge entry. The moment coefficient grows almost linearly with δ, at least for small values, and the growth rate for $\alpha = 60^\circ$ is larger than that for $\alpha = 30^\circ$. This is due to the strong nonlinear effects that occur at small deadrise angles, which give rise to very large pressure peaks.

There are two different effects limiting the maximum heel angle. The first limitation has a physical background, being related to the occurrence of flow separation from the wedge apex, as experimentally observed (Judge *et al.* 2004). As $\beta_R \to \pi/2$, the pressure on the left-hand side pushes the fluid toward the right and, for large β_R, separation takes place at the wedge apex. Correspondingly, as the heel angle grows, the total force on the right-hand side C_{nR} progressively diminishes: we assume the point of separation as that where the force C_{nR} crosses the zero axis and becomes negative. The second limitation comes from the geometrical constraint $\beta_L > 0$ which implies $\delta < \pi/2 - \alpha$. From figure 10(*a*) it can be seen that, for $\alpha = 30^\circ$, the force coefficient on the right-hand side becomes zero when $\delta^*/\pi \sim 0.1$, which corresponds to $\beta_R^* \sim 0.43\pi$. In the case of the blunt wedge, $\alpha = 60^\circ$, we see from figure 10(*b*) that, up to the geometrical limitation $\delta = \pi/6$, the force on the right-hand side remains positive, thus indicating that flow separation does not occur, at least for the vertical water entry considered in the present calculations.

It is worth remarking that there is no experimental evidence which can confirm the criterion we proposed to signify the occurrence of flow separation. To our knowledge, the only experimental work aimed at evaluating limit conditions for flow separation is by Judge *et al.* (2004). In their experiments they used a wedge with $\alpha = 53^\circ$ and heel angle ranging from 0 to 34°. The role played by the horizontal component of the entry velocity has been investigated as well. Experimental measurements show that, for the vertical water entry, flow separation does not occur for such wedge, even at the largest heel angle, $\delta = 34^\circ$. In presence of the horizontal velocity component, separation is found at some heel angle which depends on the horizontal velocity

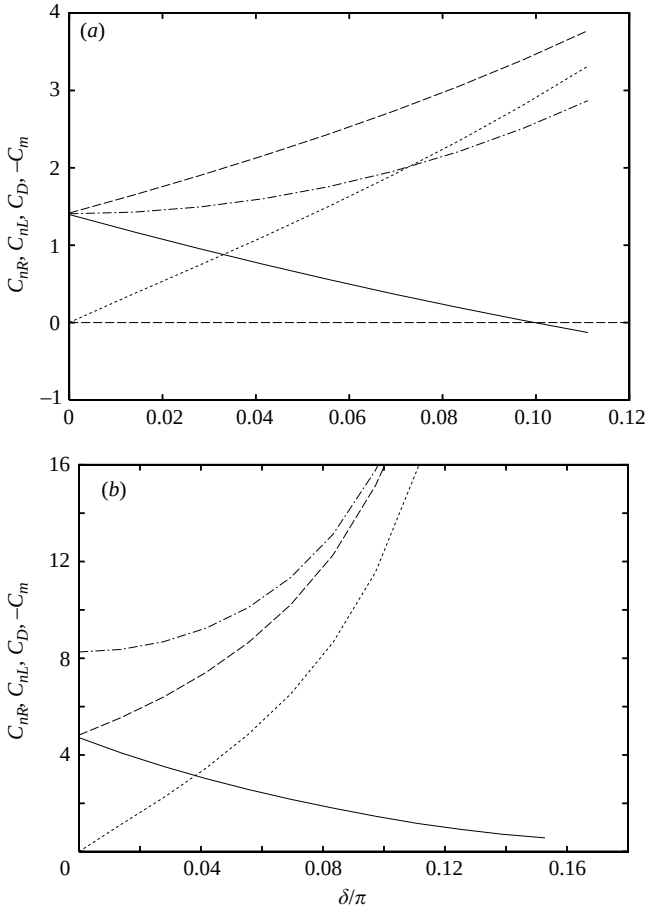

FIGURE 10. Effect of the heel angle on non-dimensional coefficients: normal force on the right-hand side C_{nR} (solid), normal force on the left-hand side C_{nL} (dashed), total vertical force C_D (dash-dot) and moment coefficient C_m (dotted). Results are shown for wegdes with (*a*) $\alpha = 30^\circ$ and (*b*) $\alpha = 60^\circ$.

component. At first separation occurs with the jet tip remaining attached to the wedge surface. Starting from these conditions, a further increase of δ leads to the complete separation of the flow from the wedge side.

With the aim of evaluating the separation-free limits for the vertical water entry of asymmetric wedges, calculations are performed for several wedge angles α and heel angles δ and the value δ^* corresponding to zero force on the right-hand side of the wedge is plotted versus α in figure 11. It is found that the relation $\delta^*(\alpha)$ is approximately linear with $\delta^* \simeq 0.62\,\alpha$. For $\alpha > 55^\circ$ ($\alpha/\pi > 0.30$) the normal force acting on both wedge sides is positive for any heel angle below the geometrical constraint. This result agrees with that found in Judge *et al.* (2004), who did not find flow separation for the vertical water entry of a wedge with $\alpha = 53^\circ$. The maximum heel angle before flow separation occurrence has also been evaluated by de Divitiis & de Socio (2002). However, due to the assumptions made in their model, they predicted a much smaller range for the separation-free region.

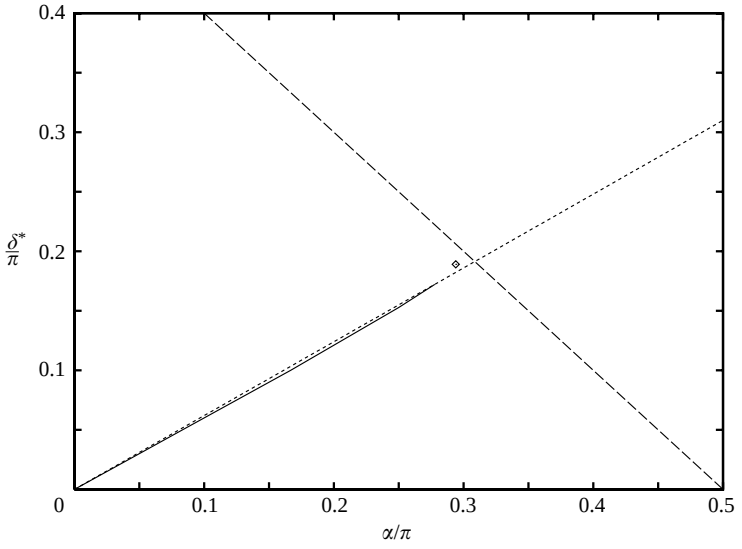

FIGURE 11. The heel angle $\delta*$ corresponding to zero force on one wedge side versus the wedge angle α. The separation-free region lies below the solid line. This line can be approximated by $\delta* \simeq 0.62\alpha$ (dotted). The dashed line corresponds to the geometrical constraint $\beta_L = 0$ while the diamond shows to the separation-free condition experimentally found in Judge *et al.* (2004).

5. Conclusions

The self-similar flow generated by the vertical water impact of asymmetric wedges has been analytically solved. The theoretical approach is based on the construction of the complex velocity potential in the parameter plane including the modulus and the angle of the velocity as functions of the arclength along the free surface. The problem is reduced to a system of an integral and an integro-differential equation with respect to these functions which is solved by applying the Hilbert transform.

It is shown that, during the vertical impact of an asymmetric wedge, one side of the wedge pushes out the liquid toward to the other side. This affects the free surface elevation, decreasing the level on the side with the lower deadrise angle and, correspondingly, increasing the level on the other side. With respect to the symmetric solution, asymmetry leads to a reduction of the pressure peak on the side with the smaller deadrise angle and a growth of the pressure peak on the opposite side. Furthermore, the occurrence of a stagnation point on the less inclined side of the wedge has been highlighted and the pressure about it has been discussed.

Limit conditions beyond which flow separation from the wedge apex may occur have been evaluated on the basis of the total normal force acting on the wedge sides. Within the region of attached flow, parametric dependences of the contact angles at the intersections of the free boundary and the wedge, the pressure distribution, and the force and moment coefficients have been provided.

Yu.A.S. gratefully acknowledges the Consiglio Nazionale delle Ricerche of Italy which partially supported the study under the NATO Grant Bando N. 217.35 S - 2004.

REFERENCES

Armand, J. L. & Cointe, R. 1987 Hydrodynamic impact analysis of a cylinder. *J. Offshore Mech. Artic Engng* **9**, 237–243.

Battistin, D. & Iafrati, A. 2004 A numerical model for the jet flow generated by water impact. *J. Engng Maths* **48**, 353–374.

Borg, S. F. 1957 Some contributions to the wedge-water entry problem. *J. Engng Mech. Div. Proc. ASCE* **83**, 1–28.

Chekin, B. S. 1989 The entry of a wedge into incompressible fluid. *Prikl. Matem. Mekhan.* **53**, 300–307.

Cointe, R. 1991 Free surface flows close to a surface-piercing body. *Mathematical Approaches in Hydrodynamics* (ed. T. Miloh), pp. 319–334, SIAM, Philadelphia, USA.

de Divitiis, N. & de Socio, L. M. 2002 Impact of floats on water. *J. Fluid Mech.* **471**, 365–379.

Dobrovol'skaya, Z. N. 1969 Some problems of similarity flow of fluid with a free surface. *J. Fluid Mech.* **36**, 805–829.

Faltinsen, O. M., Landrini, M. & Greco, M. 2004 Slamming in marine applications. *J. Engng Maths* **48**, 187–217.

Fraenkel, L. E. & Keady, G. 2004 On the entry of a wedge into water: The thin wedge and an all-purpose boundary-layer equation. *J. Engng Maths* **48**, 219–252.

Fraenkel, L. E. & McLeod, J. B. 1991 Some results for the entry of a blunt wedge into water. *Phil. Trans. R. Soc. Lond.* A**355**, 523–535.

Garabedian, P. R. 1953 Oblique water entry of a wedge. *Commun. Pure Appl. Maths* **6**, 157–165.

Greenhow, M. 1987 Wedge entry into initially calm water. *Appl. Ocean Res.* **9**, pp. 214–223.

Gurevich, M. I. 1965 *Theory of Jets in Ideal Fluids*. Academic.

Helmholtz, H. 1868 Ueber discontinuirliche Flussigkeitsbewegungen. *Monasber. Berlin Akad.* 215–228.

Howison, S. D., Ockendon, J. R. & Oliver, J. M. 2004 Oblique slamming, planing and skimming. *J. Engng Maths* **48**, 321–337.

Howison, S. D., Ockendon, J. R. & Wilson, S. K. 1991 Incompressible water entry problems at small deadrise angles. *J. Fluid Mech.* **222**, 215–230.

Iafrati, A. 2000 Hydrodynamics of asymmetric wedges impacting the free surface. *Proc. of the ECCOMAS Conference* (ed. E. Oñate), CIMNE, Barcelona (Spain), on CD-rom.

Judge, C., Troesch, A. W. & Perlin, M. 2004 Initial water impact of a wedge at vertical and oblique angles. *J. Engng Maths* **48**, 279–303.

von Kármán, T. 1929 The impact of seaplane floats during landing. *NACA TN* 321.

Keady, G. & Fowkes, N. D. 1998 The vertical entry of a wedge into water: integral equations and numerical results. *Proc. Engng. Math. and Appl. Conf.* (ed. E. O. Tuck & K. Scott), pp. 277–280. Institute of Engineers, Adelaide (Australia).

Kirchhoff, G. 1869 Zur Theorie freier Flussigkeitsstrahlen. *J. Reine U. Angew. Math.* **70**, 289–298.

Korobkin, A. A. 1988 Inclined entry of a blunt profile into an ideal fluid. *Fluid Dyn.* **23**, 443–447.

Korobkin, A. A. & Peregrine, D. H. 2000 The energy distribution resulting from an impact on a floating body. *J. Fluid Mech.* **417**, 157–181.

Mackie, A. G. 1969 The water entry problem. *Q. J. Mech. Appl. Maths* **22**, 1–17.

Mei X., Liu Y. & Yue D. K. P. 1999 On the water impact of general two-dimensional sections. *Appl. Ocean Res.* **21**, 1–15.

Scolan, Y. M., Coche, E., Coudray, T. & Fontaine, E. 1999 Etude analytique et numérique de l'impact hydrodynamique sur des carénes dissimétriques. *Proc. 7th Journees de l'Hydrodynamique.* (ed. B. Molin), pp. 151–164. Group ESIM, Marseille (France).

Toyama, Y. 1993 Two-dimensional water impact of unsymmetrical bodies. *J. Soc. Naval Arch. f Japan* **173**, 285–291 (in Japanese).

Tulin, M. P. 1957 The theory of slender surface planing at high speeds. *Schiffstechnik* **4**, 125–233.

Vorus, W. S. 1996 A flat cylinder theory for vessel impact and steady planing resistance. *J. Ship Res.* **40**, 89–106.

Wagner, H. 1932 Über Stoßund Gleitvorgänge an der Oberfläche von Flüssigkeiten. *Z. Angew. Math. Mech.* **12**, 192–215.

Wu, G. X., Sun H. & He, Y. S. 2004 Numerical simulation and experimental study of water entry of a wedge in free fall motion. *J. Fluid Struct.* **19**, 277–289.

Xu, L., Troesch, A. W. & Vorus, W. S. 1998 Asymmetric vessel impact and planing hydrodynamics. *J. Ship Res.* **42**, 187–198.

Zhao, R. & Faltinsen, O. M. 1993 Water entry of two-dimensional bodies. *J. Fluid Mech.* **246**, 593–612.

Zhukovskii, N. E. 1890 Modification of Kirchoff's method for determination of a fluid motion in two directions at a fixed velocity given on the unknown streamline. *Math. Coll.* **15**.